LONDON, METEOROLOGICAL OFFICE.
Met.O.19 Branch Memorandum No.93

Ground truth confirmation and theoretical limits of an experimental VLF arrival time difference lightning flash locating system.

07971287 FH5B

Met O 19 BRANCH MEMORANDUM No. 93

GROUND TRUTH CONFIRMATION AND THEORETICAL LIMITS OF AN EXPERIMENTAL VLF ARRIVAL TIME DIFFERENCE LIGHTNING FLASH LOCATING SYSTEM

by

Dr. A. C. L. Lee

Met O 19
(Satellite Meteorology)
Meteorological Office
London Road
BRACKNELL
Berks RG12 2SZ

27 November 1987

Ground Truth Confirmation and Theoretical Limits of an Experimental VLF Arrival Time Difference Lightning Flash Locating System

By A. C. L. Lee

Meteorological Office, Bracknell

SUMMARY

During trials of a VLF Arrival Time Difference (ATD) technique for long range lightning flash location, an apparently well organised and isolated flash sequence was located. Internal ATD evidence suggests flashes were located at a thousand kilometer range to within 5 km, and "ground truth" based on synoptic/mesoscale considerations, observer reports, and lightning damage claims confirms this. In addition, elimination of potential systematic effects from the internal evidence, supported by apparent storm movement over a 3 km path, indicates that the relative flash location error was 880 m. The nature of VLF lightning flash observation is examined, and shown to be consistent with errors even smaller than this.

1. Introduction

Lee (1986a) describes an experimental system for lightning flash location at ranges up to several thousand kilometres, and compares it with other systems. This system exploits the differences in arrival times of lightning-originated radio atmospherics ("Sferics") in the Very Low Frequency (VLF) band at a network of "Arrival Time Difference" (ATD) Outstations deployed over the United Kingdom and Mediterranean. The flash location is inferred from measured ATD values using methods analogous to hyperbolic navigation techniques.

The cited paper describes the system's principles, presents its accuracy as contours of location error over a "Service Area" from 40°W to 40°E, 30°N to 70°N if an ATD root mean square (RMS) error of 25 μs is assumed, and shows by a statistical technique that RMS errors as low as 3.3 μs were achieved experimentally implying a proportionally reduced flash location (or "fix") error. At this high accuracy no other operational meteorological system can provide an independent comparison.

This paper explores a case study for "ground truth" comparison. Although ATD precision is lower than described above, ground truth is more accurate than has been reported previously and supports the internally estimated ATD error, lending credence to the statistical method. Furthermore, this study shows that the indicated scatter in flash fixing is considerably smaller (at 880 m) than absolute fix error, and that this low scatter is physically reasonable. Thus accuracy could be improved by removal of systematic effects.

The Meteorologial Office is currently deploying an ATD system as charted on Fig 4 of Lee (1986a). At the measured ATD precision, this implies fix errors of 0.7-10 km over most of the Service Area. Unfortunately, the operational system cannot confirm this potential as communications costs are reduced by degrading ATD errors to around 5-8 μs. Thus the statistical results (Lee, 1986a), and the present study, will probably be the sole evidence that removal of this degradation could facilitate higher accuracy if required. The operational system, its requirements and limitations, and comparison with other systems, is described in Lee (1986b).

2. An unusual event

During an ATD trial (Lee, 1986a), the experimental equipment was operated for short pre-arranged periods to allow comparison with another system, recording limited-rate data within ten-minute windows immediately before certain GMT hours and half-hours.

An isolated event occurred in the ATD system results for 12 July 1979 within the 1050-1100 GMT window, when several ATD fixes were observed near the Massif Central (France) at 45°04'N 03°01'E, with internal evidence supporting an ATD (timing) RMS error of 5.0 μs, discussed below. This value is based on only 31 flashes, but represents a claim for less ATD precision than was demonstrated in Lee's (1986a) "Trial (a)" results from 1085 flashes which gave 3.3 μs error, so is not unreasonable for accurate clock alignment. With 5.0 μs

error, and the trial Outstation deployment. Fig 3 of Lee (1986a) predicts an absolute location error here of 4.8 RMS km. The fixes appeared organised, with unusually powerful Sferics, suggesting some prospect of identifying and locating the storm to provide an accurate fix comparison.

3. The meteorological situation

The meteorological situation featured a depression centred over central France close to the location described above. By 0900 GMT thunderstorms had already been observed to the west of the ATD "event", as described below.

Fig 1 shows the local 1200 GMT chart analysed from French SYNOP reports. Between 44-46°N and 01-05°E height contours are drawn at 1220, 1525, and 1830 metres: note the Plomb du Cantal at 45°04'N 02°45'E, and the South-West facing slope of the Margeride with its North-Western end at 45°00'N 03°15'E. Wind velocity "arrows" are drawn conventionally in knots. The depression had deepened slightly, and streamlines drawn (as dashed lines) from surface wind observations indicated strong confluence (and therefore probably convergence) from the south to the east of the Cantal in the region of interest, about one hour after the observed event.

The SYNOP reports, and observer reports detailed below, report no thunderstorms to the south or south-west of the Cantal within 100 km, except shortly before the event itself. Thus during this early period the confluent airstream was

probably still stable, with convergence accentuated by funnelling of air between the Cantal and Margeride. A position between these profiles (eg the observed position of the event at 45°04'N 03°01'E) might be particularly favourable to triggering thunderstorms in this potentially unstable airstream.

Fig 1 indicates a supply of warm moist air at low levels to the event, with high (20°C) values of surface wet-bulb potential temperature. Fig 2 presents wind profiles and tephigrams for the 1100 GMT Lyon Nimes and Bordeaux radiosonde ascents. Nimes and Lyon show a wet-bulb potential temperature decreasing from the surface, and thus potential instability. Should orographic lifting raise the surface layers to the condensation level at 950-900 mb (approximately 600-1000 m), the resulting actual instability would extend up to the tropopause at around 230 mb, releasing substantial buoyancy. Both Lyon and Nimes show wind veering with height through much of the potentially convective layer, exhibiting a 30-40 knot (15-21 m s^{-1}) shear between the surface and 500 mb levels. While the profile remains stable, the topography can funnel the local air mass up the rising terrain to the south and south-west of the Cantal and Margeride, where the condensation level is easily exceeded, triggering instability. This combination suggests (Ludlam, 1980) the possible formation of an organised storm, having some persistent structure, provided a suitably located trigger exists.

Evidence presented below suggests initial instability on the Cantal, the resulting outflow spreading into the

surrounding area to trigger further activity at suitable points (Ludlam, 1980). The flow of low-level, potentially unstable air along the south-west face of the Margeride may have been deflected by the detailed profile of the Margeride towards the outflow boundary. The intersection of the outflow boundary and the feedstock air flow could well have formed a suitable trigger point for an organised storm event (Purdom 1984, 1979), as detected by the ATD system.

Thus synoptic evidence, combined with local topography, favours the outbreak of an intense event to the east of the Plomb du Cantal as observed, but the accuracy of synoptic placement is limited to around 10-20 km.

4. Mesoscale ATD data

Fig 3 shows an expanded chart, highlighting the Plombe du Cantal and Margeride through shading at 1250 m and 1500 m. ATD fixes are superimposed as numbered points surrounded by a small circle. The Flash Number refers to a chronological list of detected flashes, including those missing data through experimental limitations (Lee, 1986a) which were unfixable.

Table 1 details all ATD fixes from 0950-1130 GMT for which CRDF selections were made, and Sferics recorded at all four Outstations; listing the Flash Number, its epoch (GMT) on 12 July 1979, and ATD fix in decimal degrees. The flash RESIDUAL (ATD RMS error) is given in microseconds, together with estimated distance from 45°04'N, 03°01'E to identify

TABLE 1

Flash No.	GMT HHMM SS	ATD Location Decimal Degrees N	E	RESIDUAL μs	Distance from 45°04'N, 03°01'E km
416	0952 01	37.923	-47.262	3.6	4203
428	0955 07	45.127	2.596	0.5	34
444	0957 44	45.148	2.987	2.8	9
449	0958 26	45.168	2.984	2.5	12
450	0958 42	37.518	-42.164	4.6	3824
457	0959 33	45.146	2.646	5.2	31
459	1020 15	45.231	2.711	4.7	30
461	1020 50	44.962	2.530	6.2	40
470	1022 52	37.167	-42.280	4.1	3851
475	1023 47	45.308	2.752	0.5	34
477	1024 30	44.877	2.874	4.6	24
487	1027 17	30.231	-86.070	3.6	7635
490	1027 43	51.316	-53.772	7.1	4171
497	1028 27	45.326	2.780	11.7	34
500	1028 45	37.514	-42.202	1.9	3827
501	1028 58	44.164	0.983	4.0	190
503	1029 17	(45.235	2.241)	102.8	--
		(No resemblance to other flashes)			
519	1051 22	11.881	-55.977	1.7	6661
524	1052 14	(45.411	3.417)	279.6	--
		(No resemblance to other flashes)			
525	1052 25	46.931	34.751	0.1	2450
528	1052 50	45.058	3.005	1.4	1
533	1054 05	(45.270	2.588)	103.0	--
		(approx 45.06	3.03 if one cycle added)		
537	1054 48	45.063	3.027	2.5	1
542	1056 04	(45.301	2.622)	108.4	--
		(approx 45.06	3.03 if one cycle added)		
543	1056 24	45.067	3.017	0.8	0
545	1056 48	(45.301	2.594)	109.5	--
		(approx 45.06	3.03 if one cycle added)		
549	1057 48	45.072	3.022	10.7	1
556	1059 07	47.469	2.330	8.1	272
557	1059 14	45.080	3.041	2.9	2
561	1059 47	45.286	2.862	3.8	27
567	1120 11	30.167	-66.882	6.1	6190
568	1120 22	47.599	4.376	5.7	300
580	1121 36	44.918	3.165	2.9	20
581	1121 45	47.598	4.359	8.2	300
597	1124 17	45.220	3.199	3.7	22
604	1125 19	11.677	-57.745	1.4	6812

TABLE 2

Flash	RESIDUAL	Arrival Time Difference Values with respect to Beaufort Park (μs)		
	μs	Camborne	Gibraltar	Shanwell
528	1.4	299.4	1513.6	1901.9
533	103.0	296.8	1619.8	2009.8
537	2.5	301.5	1517.9	1900.3
542	108.4	303.9	1641.1	2014.3
543	0.8	301.3	1519.7	1902.1
545	109.5	301.7	1640.4	2015.8
549	10.7	300.0	1523.6	1892.3
557	2.9	304.1	1529.8	1899.5
561	3.8	304.8	1649.2	1900.2

"event" flashes and indicate their isolation. RESIDUAL values exceeding 40 μs indicate mis-matches of at least one cycle (around 110 μs) in aligning Sferic waveforms, producing relatively large location errors (Lee, 1986a); these locations are in parenthesis, and the event distance omitted. The RMS RESIDUAL, calculated over the 31 correctly-matched Table 1 flashes, is 5.0 μs.

Flashes 533 542 and 545 occurred during the "event", but their records indicate equipment overload, leading to mis-match. Table 2 lists Flash Number, RESIDUAL, and ATD values for these flashes, and for the others that occured close to 45°04'N, 03°01'E between 1050-1100 GMT. Camborne ATD values are almost identical, and the excessive RESIDUAL was apparently due to a single cycle slippage of approximately 110 μs in two of the ATD values. Adjustment by this amount would give fixes at approximately the event location with a 10-20 μs RESIDUAL. Thus these flashes were almost certainly part of the intense event, although their precise location is unknown.

Thus, of 13 four-station flashes detected between 1050-1100 GMT, eight are probably within 5 km of 45°04'N, 03°01'E, with five within 2 km. This density is highly unusual for the low experimental selection rate, Table 1 periods 0950-1030 and 1120-1130 being more typical. The high Sferic intensities and multiple coincident locations suggest a severe and organised storm which may have been noted, even in this storm-prone region.

All Table 1 low-RESIDUAL fixes within Fig 3's area are plotted. The observed activity is isolated, with the

closest remaining flashes hundreds of kilometers away. Time sequences are evident through Table 1 and the Flash numbers: 416-457 (0950-1000 GMT, one hour before the event) are depicted as "open" points. This early activity occurred near the Cantal's high ground, presumeably triggered by orographic lifting. Flashes 459-503 (1020-1030, the window immediately before the event) depict the storms spreading in the downflow around the Cantal, with most activity to the north-east lee. Flashes 519-561 (1050-1100) include the "event", with locations bunched in the confluence area between the Cantal and Margeride, and a single flash 561 to the east of the previous area. Finally, Flashes 567-604 (1120-1130) include the two most eastern locations, while later activity is also to the east. The general picture agrees quite plausibly with the synoptic situation, showing a general easterly movement with a concentration of activity in the confluent area.

5. Observer evidence

Useful observer data were supplied by the Meteorologie Nationale from logs of the Aurillac and Cantal departments, although the timing was not really adequate, and daytime observer location of storms is probably accurate to only 2-3 km. The following describe all reports for the day, in chronological order, as plotted on Fig 3:

(a) 0900 GMT: strong storm at Le Fau. This is before the period, but is the first report in this area, and describes

early Cantal activity.

(b) 0930 GMT: clap of thunder heard at Aurillac town. An early report, west of the general area.

(c) 0930-1100 GMT: storm at Montgreleix. The former time falls outside the period, but the latter agrees with Flashes 475 and 497 to the north east of the Cantal (1024 and 1028 GMT respectively), and Flash 561 in the later observation window (1100).

(d) 0945-1045 GMT: storm observed from Aurillac Tronquieres (meteorological station) forming to the north-east. This appears to be the same observation as (b).

(e) 1000-1030 GMT: storm at Le Claux. This agrees closely with the early Flashes 428 and 457 on the Cantal (0955 and 1000 GMT respectively), and with Flash 459 (1020 GMT, next ATD window) to the north-east. The activity may have moved near Le Claux at about the reported time.

(f) 1000-1100 GMT: storm reported at Le Falgoux on the Cantal. This coincides precisely with Flashes 428 and 457 (0955 and 1000 GMT respectively).

(g) 1000-1100 GMT: storm at Mandailles. This lies between the area of Flashes 428/457 and Flash 461 to the SSW (0955, 1000, and the next observation window at 1021 GMT respectively), suggesting the downflow triggering activity in the surrounding area.

(h) 1000 onwards: storm at Vic sur Cere "during the afternoon". 1200 local time corresponds to 1000 GMT, so the storm probably occurred after 1000. Flash 461 (1021 GMT) coincides.

(i) 1000 onwards: storms and heavy showers at Saint Illide

"during the afternoon". The ATD system did not detect coincident flashes, although the sample rate is low.

(j) 1000 onwards: storm reported at Deux Verges "during the afternoon". The report's position suggests a spread of activity from the Cantal to the east. Flash 477 (1024 GMT) lends some support.

(k) 1100-1230: storm at Talizat. This area is to the NE of Flashes 528/537/543/549/557, which occured between 1053-1059 GMT. The progression of ATD fixes (discussed below) implies that the storm may have passed 2 km or so to the south and east of Talizat, and that timing may have been as reported.

(l) 1000 GMT onwards: "very violent storm" reported at Lastic "during the afternoon". The track of Flashes 528-557 described above may have continued and developed during the ATD observations gap from 1100-1120 GMT, with activity spreading to include Lastic. It is frustrating to find no ATD observations for Lastic itself, but this gap and the low sample rate may explain this; there were no damage claims at Lastic, discussed below. Flash 597 (1124 GMT) appears to lie further along this track, and to have approximately the correct timing.

(m) 1100 GMT: "storm" at Ruynes en Margeride. This suggests continuing easterly spread, as indicated by Flash 580 (1121 GMT).

(n) 1150 GMT: "storm" at Massiac. This observation continues the easterly trend. The flash sequence from 528 (1053 GMT) through 557 (1059 GMT) to 597 (1124 GMT) is not inconsistent with this report.

(o) Time not recorded: storm reported at Marcenat, to the

north-east of the Cantal. This agrees with Flashes 497 and 561.

The coincidence between audio/visual observations and ATD fixes is remarkable, given the recognised limitations of observer reports. The only other observer reports in the general area were at Le Puy-Chadrac (45°05'N, 03°46'E) from 1345 to 1610 GMT, and at Clermont-Ferrand-Aulnat (45°48'N, 03°10'E) from 1555 to 1710 GMT. Note that observer reports indicate that activity was isolated to approximately the regions and times indicated by ATD reports.

6. Physical evidence

The Meteorologie Nationale also provided an Assurance Company report detailing lightning damage claims received for that day in the area. No timing information was available, and locations may merely indicate the nearest town, but these help fill observer gaps. From the earlier evidence there should be rough timing coincidence between damage and ATD locations. Details are ordered from west to east, for all events on the area defined by Fig 3; in practice little else was reported. A seperate entry is given for each reported damage incident:

(a) Laroquebrou: Cow.

(b) Rouziers: Electrical appliance motor.

(c) Arfrajon-sur-Cere: Electrical appliance motor.

Cow.

(d) Sansac Veinazes: "Electric Shepherd".

(e) Vezac: Refrigerator.

Electrical appliance motor.

(f) St Projet de Salers: "Electric Shepherd".

(g) Polminac: Bull calf.

(h) St Julien de Jordanne: Motor and water pump.

Damage reports (a) to (h) are all to the south-west of the Cantal.

(i) Chanterelle: Cooker.

This report is in the area to the north-east of the Cantal.

(j) Valuejols: Television.

Lies to the north-west of the ATD reported storm path.

(k) Neuveglise: Television.

Cow.

General activity to the south-east of the Cantal.

(l) Joursac: Cow.

Activity to the north of the ATD reported storm path.

(m) St Remy de Chaudes Aigues: Foal.

General activity to the south-east of the Cantal.

(n) Roffiac: Refrigerator.

This location, at 45°03'N 03°03'E, lies just 2 km to the south-east of the ATD reported storm path.

(o) Talizat: Television

Two televisions plus radio mast.

Washing machine motor.

Cow.

Taligat lies approximately 3 km to the north-west of the continuation of the ATD reported storm path. Although the observer here merely reported "storm from 1100-1230 GMT", the number of damage reports (compared with none at Lastic) lends support to the ATD position of the storm path. The intensity of the storm damage to the west and north of Lastic suggests that it might have been heard there.

(p) Ferrieres St Mary: (Item unidentified).

(q) Charmensac: Three cows.

(r) Laurie: Electrical appliance.

(s) Coren: (Item unidentified).

(t) St Mary Le Plain: Refrigerator and cooker.
Electrical appliance motor.

(u) Massiac: Electrical appliance.

(v) La Chapelle Laurent: Refrigerator thermostat.

All the damage reports from (p) to (v) suggest a continuation and spreading of the storm path.

This extra evidence agrees with the ATD reports, and complements the meteorological observations. These data are for the whole day, although the noticeably dense and intense damage reports coincide with the path of the ATD "event", making coincidence likely.

7. Absolute ATD location accuracy

The synoptic analysis and human observations described

above give good agreement, and confirm the ATD activity pattern. Coincidences between audio/visual sightings and ATD fixes, particularly on the Cantal and to its NE, are good when event timings are considered. The damage claims support this pattern, and also the ATD "event" storm progression that is - at least initially - highly intense and organised, although lack of ATD data between observation windows is frustrating. Its coincidence at Roffiac is excellent, as is its extended path with the intense damage report at Talizat, suggesting confirmation of some ATD data to an absolute accuracy better than the 4.8 km prediction from RMS RESIDUAL, although it is impossible to equate individual strokes with damage or observations. Lee (1986a) claims higher fix precision for this area (from RESIDUAL), but this paper gives a much closer agreement with "Ground Truth" now that it has been possible to locate the latter in more detail.

8. Relative ATD location accuracy.

(a) Introduction

Lee (1986a, Sections 5(e,f)) notes that the time-dimensioned RMS RESIDUAL used above gives a pessimistic measure of potential location accuracy. It includes systematic contributions from experimental timescale alignment errors, and from propagation effects not accurately covered in the "zero-order correction" used to calculate Sferic phase velocity. Random ATD errors require optimal

fix algorithms which weight ATD differences by prior standard deviations, but RESIDUAL assumes these are "unity" giving values biased towards larger errors.

In this section a modified use of RESIDUAL eliminates systematic effects (estimates relative errors) by extending the adjustable degrees of freedom (DOF) to include systematic offsets. A stepwise analysis of variance using the F-statistic shows the above data sample has a mixed relative location error population - a normal distribution with 1.9 km errors, and a proportion of outliers significant at the 0.1% level. In a further modification, the different ATD variances at the non-Reference Oustations are analysed, reducing the estimated normal location error to 0.9 km. In both cases, the size and sign of the systematic offsets are compatible with known propagation effects.

(b) Elimination of systematic offsets

Experimental timescale errors were excessive compared to those for an operational system, but for flashes observed over a limited period misalignments should be correctable by adding constant "timing" Offsets to ATD values with respect to Beaufort Park for Camborne Gibraltar and Shanwell (CGS). For such flashes observed from a small area, similar flash-to-flash propagation biases result from similar source waveforms, correctable by adding constant "propagation" Offsets to ATD values. The sum of these Offsets at each of the non-reference Outstations may be estimated by a minimisation over several flashes with respect to Offsets as well as flash coordinates. In practice, for small flash

areas Offset estimates are ill conditioned, but the minimisation estimates relative ATD errors accurately.

Using Lee's (1986a, Appendix D) notation, RESIDUAL is re-cast into a chi-square form, including Offsets O, and summing over n flashes each of m ATD values:

$$\chi^2 = \sum_{s=1}^{n} \{(m-2)\,\mathrm{RESIDUAL}^2(\phi_s, \lambda_s)\}$$

Subscript CAP "M"

$$= \sum_{s=1}^{n} \left\{ \sum_{r=1}^{m} [\{ATD_{TH}(r, \phi_s, \lambda_s) - ATD_M(r) - O(r)\}/\sigma(r)]^2 \right\} \quad (1)$$

$$\chi^2 = n(m-2) - k \qquad k = 0, \text{ if } O(r) \text{ are prior values} \quad (2)$$

$$= m, \text{ if } O(r) \text{ are DOF}$$

Eqn (1) relates χ^2 to the flash coordinates ϕ, λ and the Offsets O through the theoretical (TH) and measured (M) ATD values. If the ATD standard deviations $\sigma(r)$ are prior values then χ^2 is minimised with respect to the coordinates, and also the Offsets if these are allowed degrees of freedom rather than prior values. Alternatively, $\sigma(r)$ values may be constrained by a prior relation with one DOF (eg. equal), to be minimised with respect to the other DOF in eqn (1), with χ^2 set to its expectation of the total remaining DOF, as defined in eqn (2).

With O(r) adjusted to eliminate systematic effects,

Table 3: F-Ratios for Flashes near 45° 04'N, 03° 01'E
Fixed using equal ATD Standard Deviations

Degrees of Freedom (DOF)	17	14	12	11	10	9
			21.35(497)	27.95(497)	32.94(497)	38.33(497)
				21.94(549)	25.98(549)	30.36(549)
0.1% Sig	15.72	17.14	18.64	19.69	21.04	22.86
			16.62(549)			
2.5% Sig	6.04	6.30	6.55	6.72	6.94	7.21
	---	---			5.02(461)	6.16(461)
	5.45(497)	5.22(497)				
	4.54(549)					
5.0% Sig	4.45	4.60	4.75	4.84	4.96	5.12
		3.94(549)		4.00(461)		3.37(457)
10% Sig	3.03	3.10	3.18	3.23	3.29	3.36
	1.50(461)		---	---	2.65(457)	2.37(459)
			2.74(461)	2.03(457)	---	---
			1.88(428)	1.84(428)	1.81(459)	2.11(477)
					1.79(428)	1.71(428)
25% Sig	1.42	1.44	1.46	1.47	1.49	1.51
		1.05(428)				
50% Sig	0.475	0.479	0.484	0.486	0.490	0.494
S Dev (μs)	5.03	3.41	1.88	1.70	1.60	1.50
RMS km	4.85	3.28	1.81	1.64	1.54	1.45

location errors computed by Monte-Carlo methods from $\sigma(r)$ give the remaining (random) relative location errors. Should systematic effects not be constant as modelled above, $\sigma(r)$ is increased, ensuring a pessimistic estimate of relative location error.

From Table 1, all 17 flashes with RESIDUAL below 40 μs and within 45 km of 45°04'N, 03°01'E were selected. Equal $\sigma(r)$ were minimised with $O(r)$ zero, implying 17 DOF as m=3. The resulting $\sigma(r)$ are the RMS time-dimensioned RESIDUAL over these flashes, ie. 5.03 μs, corresponding to 4.85 RMS km (absolute) location accuracy in this area.

The selected RESIDUALs in Table 1 feature occasional large values, suggesting some non-random complication causing possible outliers from a chi-square distribution. Thus a one-sided F-Test of the null hypothesis "None of the 17 selected flashes has unusually large ATD variance" was applied by dividing χ^2/DOF for each flash (with sample-fitted $\sigma(r)$, and $O(r)$ as prior values implying (m-2) DOF) by χ^2/DOF for the sample (defined as unity by eqns(1) and (2)). The highest F-Ratios are ranked in Table 3 with identifying flash numbers in parentheses under "17 DOF" below the dashed line, and $\sigma(r)$ and the implied (absolute) location accuracy; together with F-Ratios for the sample DOF at various one-sided significance levels (Pearson and Hartley, 1976). No flash χ^2 exceeds that expected at the 2.5% significance level, indicating little evidence of departure from normal ATD distribution. The minimisation was repeated, but with $O(r)$ as adjustable DOF to obtain relative location errors, reducing the remaining DOF to 14; results are displayed under

"14 DOF". The estimated σ(r) and (relative) location errors are reduced, and the highest F-ratios for the selected flashes still lack significance.

The stepwise analysis was continued by rejecting the highest F-Ratio flashes 497 and 549, and minimising O(r) over the remaining flashes, with results shown under "12 DOF" below the dashed line; F-Ratios for the rejected flashes are shown above. Flash 497 lies well outside the 0.1% significance level, with 549 almost there - strong statistical evidence for rejecting the null hypothesis that these flashes form part of the remaining normal population. The normal population σ(r) and relative location errors are reduced to 1.88 μs and 1.81 km respectively. The fitted O(r) for 12 DOF , in order CGS, are -0.582 0.043 -2.999 μs. With 14 DOF, the abnormal flashes perturbed O(r) to -0.777 0.056 -3.888 μs, a perturbation comparable with σ(r) which increased χ^2 for the normal population, diluting the F-Ratio discrimination.

Results for sucessively smaller DOF are shown in Table 3, and their variances (normalised by the 12 DOF variance) are plotted in Fig 4 as a function of reducing DOF. Initial variance reduction is rapid, flattening out sharply at 12 DOF, implying that evidence for rejecting the null hypothesis is slight below this level. The tabled F-Ratios for flashes other than 497 and 549 confirm this view.

(c) Inclusion of ATD variance

The above estimate ignores known differences in ATD variance. The distances from these flash locations to

Table 4: F-Ratios for Flashes near 45° 04'N, 03° 01'E
Fixed using ATD Standard Deviations in the Ratio 1.51:3.11:3.47

Degrees of Freedom (DOF)	17	14	12	11	10	9
			21.76(497)	27.93(497)	32.98(497)	38.45(497)
			17.07(549)	22.03(549)	26.16(549)	30.63(549)
0.1% Sig	15.72	17.14	18.64	19.69	21.04	22.86
2.5% Sig	6.04	6.30	6.55	6.72	6.94	7.21
						6.12(461)
	---	---				
	5.45(497)	5.20(497)				
	4.56(549)					
5.0% Sig	4.45	4.60	4.75	4.84	4.96	5.12
		3.95(549)		3.91(461)	4.94(461)	3.37(457)
10% Sig	3.03	3.10	3.18	3.23	3.29	3.36
	1.48(461)		---	---	2.63(457)	2.37(459)
			2.81(461)	2.00(457)	---	---
			1.80(428)	1.85(428)	1.80(459)	2.13(477)
					1.78(428)	1.67(428)
25% Sig	1.42	1.44	1.46	1.47	1.49	1.51
		1.05(428)				
50% Sig	0.475	0.479	0.484	0.486	0.490	0.494
SD Cam (μs)	2.23	1.51	0.84	0.75	0.71	0.67
SD Gib (μs)	4.59	3.11	1.72	1.55	1.45	1.37
SD Shan (μs)	5.12	3.47	1.92	1.73	1.62	1.53
RMS km	2.35	1.59	0.88	0.79	0.74	0.70

Beaufort Park, Camborne, Gibraltar, and Shanwell are 757, 848, 1215, and 1330 km respectively, over comparable propagation paths. ATD values for CGS are computed by correlation of their received waveforms with the reference received at Beaufort Park. As the propagation path increases from that to Beaufort Park, the waveforms differ increasingly from the reference, reducing the correlation peak and progressively sensitising ATD to additive noise. Thus the ATD $\sigma(r)$ should be least for Camborne and greatest for Shanwell. The signal to noise ratios (SNRs) from the ATD extraction process (Lee, 1986a; Appendix C) confirm this. With Camborne SNR designated 0 dB for each flash, the mean SNRs (over the 15-flash selection for 12 DOF) at Gibraltar and Shanwell were -6.2 and -7.2 dB respectively, with standard errors of 1.6 dB. Assuming that random ATD errors are caused by additive noise with these relative SNRs (a reasonable assumption for a range of scenarios) then we may constrain $\sigma(r)$ for CGS to the relative ratios 0.84:1.72:1.92 respectively.

The analysis was repeated, but with $\sigma(r)$ values constrained as described, and minimised as a single DOF. Resulting F-Ratios and significances are listed in Table 4. They are almost identical with Table 3 results, and the variance plot is indistinguishable from Fig 4, confirming 12 DOF (ie. excluding 497 and 549) as the best estimator for the normal population. This implies $\sigma(r)$ of 0.84, 1.72, and 1.92 μs respectively, which a Monte-Carlo technique maps to a relative location error of 0.88 km. The corresponding $O(r)$ were -0.531, 0.035, and -2.955 μs.

(d) Comparison with theoretical propagation effects

The above alternative assumptions produced similar O(r) estimates. Camborne and Gibraltar Offsets are ill-conditioned because the flashes lie near the Shanwell to Beaufort Park baseline extension, but this geometry provides a good estimator for Shanwell's Offset, measured at -3 μs. A path-averaged Event-to-Shanwell Sferic phase velocity smaller than for Event-to-Beaufort Park by around 0.0007c (c is free-space light velocity) would explain this value. In earth-ionosphere spherical wave-guide terms (after Watt, 1967), the first mode phase velocity is approximatly 1.0035c for a south-to-north day land path at 45° latitude at 9.76 kHz. This is increased by approximately 0.0004c for an east-to-west path by the geomagnetic anisotropy, partially explaining the Offset. Lightning sources excite additional higher-order modes which attenuate rapidly, but remain significant at ranges below 1000 km or so, and exhibit phase velocities exceeding 1.04c. Thus the (multi-mode) short range phase velocity is larger (cf assumed Sferic velocity of 1.0040c; Lee, 1986a) and more variable than long range (single-mode) velocity. This reduces path-averaged velocity for the long Event-to-Shanwell path, augmenting the anisotropic Offset. Thus the -3 μs value is theoretically plausible on the basis of propagation alone.

The timescale misalignment portion of O(r) is unknown, but the above discussion indicates systematic propagation effects comparable with O(r), and larger than residual ATD scatter, explaining the substantial reduction from 4.58 km absolute

error to 0.88 km relative error. A multi-frequency propagation model could correct wave-shape pairs to an intermediate range before correlation to alleviate this "propagation-Offset", and the differentially distorting effects which reduce the correlation peak and sensitise ATD to additive noise.

(e) Some concluding points

The normal relative location error in this area for the trial geometry may have been as low as 0.88 RMS km, depending on the relative distribution of $\sigma(r)$. Outliers with substantially larger errors existed, but were detectable by analysis of variance after removal of systematic effects. Systematic propagation effects were larger than random errors, explaining the substantial improvement from a 4.58 km absolute location error, so that incorporation of a propagation model could improve absolute location accuracy.

The above calculations required double precision arithmetic. The seven significant digit arithmetic used for trial analysis (Lee, 1986a) gives adequate fix positions, but roughens the RESIDUAL surface explored by the minimiser which finds a local "pit" (near the global minimum) which is typically 0.1-0.3 μs smaller than the true value. This had little impact on trials analysis where RESIDUAL exceeded 3.3 μs, but is important for the present study of small values.

9. Microscale study of the ATD "Event"

The "Event" flashes 528 537 543 557 and 549 are plotted on the left of Fig 5 relative to the mean of the first four positions (549 is less accurate). Separate plots are superimposed for each of the DOF in Tables 3 and 4, but only different $\sigma(r)$ selections are distinguishable; Table 4 locations are marked with a cross of radius 440 m - half the normal location error.

Outlier 549 is less precisely located as $\sigma(r)$ sensitivity demonstrates. Flashes 528 543 and 557 have nearly identical return stroke waveforms, while 537 has a complex cloud to cloud waveform (for examples see Norrinder, 1954). The normal return strokes are joined by a "trajectory" marked every 20 seconds with small circles (filled every minute), for comparison with the speed scale. If the "trajectory" represents a persistent feature producing several return strokes, then it apparently moved with an initial 10 knot (5 m s^{-1}) velocity accelerating to 26 knots (13 m s^{-1}), or progressed at around 18 knots (9 m s^{-1}) with location errors that could be considerably less than twice the standard deviation of 880 m.

Fig 5's right portion maps radiosonde station positions at Bordeaux Lyons and Nimes, and the ATD Event. Hodographs scaled according to the minute (filled) dots imply wind vectors from 1000 mb every 100 mb to 300 mb, then 250 and 200 mb. The 500 mb wind at Lyons and Nimes approximates 50 knots at 212° azimuth. The trajectory implies roughly 18 knots with bearing 230° - not inconsistent with severe storm

movements, some 18° to the right of, and slower than, the midtropospheric winds (Ludlam, 1980). However, a single cell would move at the wind velocity.

This "trajectory" may fit possible persistent feature movement, although the amount of suitable data is very small. Nevertheless, the fact that realistic velocities may be reflected at all over a 3.5 km path length lends credence to the calculated relative accuracy of 880 m.

10. The "size" of the target being located.

The suggested 880 m location error is smaller than the known dimensions of a lightning flash, and may require justification.

VLF lightning sources are dominated by return strokes and K-processes rather than extensive stepped leader structures (Pierce, 1977). At extended ranges, VLF earth-ionosphere propagation enhances reception of signals for low-order ray-hop modes launched at low elevation angles (Lee, 1986a), so vertically polarised sources are enhanced, and horizontally polarised low altitude sources attenuated, through ground-reflected source images. Thus the vertical components of a tortuous discharge dominate long-range sferics, and vertical return strokes are more readily detected than K-processes in near-horizontal intra-cloud discharges.

Pierce (1977) presents the Bruce-Golde height/time distribution of return stroke current, giving constants that describe VLF sferic waveforms adequately, while Uman (1985) relates the vertical electric radiation field from an incremental return stroke height element to the derivative of its current. From these models the relative contributions of incremental return stroke elements may be illustrated by calculating the horizontally propagated vertical electric field, approximating the preferred low-elevation propagation.

The system centre frequency of 9.766 kHz is used to derive (via Laplace transform) a representative field which is plotted on an Argand diagram in Fig 6 for an integer wavelength range. This shows the complex integral (vector sum) of field amplitudes from the ground up to some marked heights for a first and a subsequent return stroke, although system mechanisms (Lee 1986a,b) ensure most selections will be "first" strokes. The total field generated between two levels is represented by the vector joining the marked levels. The model first stroke velocity decelerates, giving a natural finite Bruce-Golde channel length of 3.3 km; an arbitary limit of 7.5 km (after Master et al, 1981) was chosen for the subsequent strokes. The vertical electric field E is the integral of the "weighting function" (dE/dz) with respect to the height z, and Fig 6's height marker spacing demonstrates that the field is heavily weighted towards the lowest levels. As the weighting functions are complex they change direction, so that the total first stroke power (proportional to vector length squared) equals the power received from the lowest 1.65 km of channel: higher

levels suffer destructive interference. Similarly, 50% of power originates below 1.03 km. Corresponding figures for subsequent strokes are 2.15 km and 1.35 km.

The radiation source weighting to the lowest levels does not depend strongly on the initial assumptions. Small changes in current distribution and timing, frequency, or launch angle affect the "active" height only slightly; while earth-ionosphere propagation may be modelled as a sequence of ray-hops having properties roughly as described above. Recent return-stroke current distribution models (Uman, 1985) feature explicit breakdown and corona currents in a 7.5 km transmission line model that has been tested against sferic signals received over a wide range of frequencies and distances. Their integrals analogous to Fig 6 have similar shapes, although less curved with "active" regions extending to greater heights. Uman first (subsequent) strokes originate from the lowest 2.6 (2.6) km, with 50% power from the lowest 1.3 (1.2) km.

Thus the return stroke's active region lies within the lowest 1.5-3.0 km, of which the lowest few hundred metres is often nearly vertical (Krider et al, 1976). The horizontal distribution of weighted radiating channel should therefore be of smaller extent: much smaller than the observation wavelength (31 km), implying that the radiation source may be averaged linearly into a vertical "centre of gravity" or phase centre whose position is largely independant of observation azimuth. This is quantified below.

Consider radiators at the same height. From radiator amplitude E_0 at the origin, and E_1 at d_1 along the x axis.

SUBSCRIPT 1

the total signal observed at azimuth ϕ with phase referred to E_0's signal is proportional to $E_0 + E_1 . \exp(s.d_1 . \cos(\phi)/c)$, where s is the complex frequency and c the phase velocity. For $s.d_1/c << 1$ the exponential may be expanded to first order to give a total identical to a similarly expanded total from a single source E at d along the x axis, provided:

$$E = E_0 + E_1 \quad \text{and} \quad d = d_1 . E_1 / (E_0 + E_1).$$

This is the conventional "centre of mass" provided E_0 and E_1 are in phase. With different phases d is complex, and its imaginary part introduces a ϕ-variation, although this is small unless E_0 and E_1 are of comparable amplitude and have a substantial phase-difference. Two vertically oriented return stroke increments at the same height should exhibit similar phase as both portions originate from the same ground point, and are subject to similar velocities. Different phases may occur through near-horizontal branching, but branches probably have small vertical components. Thus return stroke components (discrete or distributed) at the same level are essentially replaceable by a single component whose complex amplitude varies little with observation azimuth.

To investigate horizontally distributed strokes, a Bruce-Golde or Uman current distribution was combined with an assumed horizontal distribution of successive vertical channel increments, to be simulated by the same current distribution in a vertical channel located at the "phase centre". The model signal phase was compared with that from the phase-centre source, and the RMS difference (over observation azimuth) minimised by fitting the phase centre

position. This RMS phase (radians) was multiplied by (observation wavelength/(2π)) to interpret its variation as an apparent return stroke phase "size" H.

Nine horizontal distributions along the x axis were modelled, having the form:

$$x = A.function(\pi.height.n/(2.channel\ height))$$

where "function" was unity for one model; and "sin" or "cos" for four models each, n being 1-4. "A" was chosen to give a total horizontal extent of "h" metres for the distribution. Detailed results are not presented here, but for Bruce-Golde or Uman, first or subsequent, return strokes H increased approximately with h^2. For an unrealistically large physical extent h of 3 km, all first strokes gave a phase size H below 100 m, with subsequent strokes below 200 m; most were a factor of 2-10 smaller. Thus the "phase image" of most return strokes, defined as a function of the entire channel, may be regarded as "vertical" with essentially negligable horizontal dimensions. There is no theoretical reason to doubt the 880-metre RMS self-consistency of individual flash locations, or its interpretation as the relative location accuracy for phase images.

11. Systematic flash progression in nature.

Precision VLF fixes demonstrating organised sequences like Fig 5 have not been reported from other systems, but comparable evidence is available by associating VLF structure

with the optical return stroke channel. Kidder (1973) used a network of motor car hub caps and automatic cameras to locate lightning return strokes with 2 km errors, and observe their sequential surface patterns. Most strokes were distributed randomly within envelopes having dimensions of 10-20 km or more, but he notes cases with systematic displacement of consecutive flashes. On 1 Dec 1970 flashes 31-35 progressed along an almost straight line of length 3 km, and then flashes 35-40 lay along an orthogonal line of length 3.5 km. On 21 Mar 1971 a sequence of ten flashes between 1946-2003 hrs (17 mins) progressed north-east along a well-defined line of length 17 km and width 1-2 km, spoiled only by flash 4 which lay 4 km off the main line. Thus systematic flash progression does occur in nature. Details of wind direction are not given, but Kidder records an isolated storm on 30 Oct 1971 where combined radar and hub-cap measurements indicate flashes occurring near the leading edge of the radar echoes and close to the highest parts, suggesting reasons for return stroke progression in an organised cell.

12. Discussion.

Trial ATD fixes were examined for consistency with local "ground truth" data. There are obvious difficulties co-locating data at megametre ranges, but a combination of synoptic, meteorological observer, topography, and damage

claims confirm the 4.8 km absolute error calculated from the 5.0 μs RMS RESIDUAL of the data. This probably represents the best long-range ground-truth confirmation for the VLF ATD principle that will conveniently be available, as the operational system sacrifices location accuracy to achieve communication economies.

Elimination of potential systematic effects (mainly due to propagation) suggests that relative location errors of 880 m were achieved. The potential for VLF ATD location to this precision is shown theoretically. Paradoxically, more precise location is possible at longer wavelengths because the overall return stroke structure is accurately averaged, giving an effective point source. An ATD system approaching this precision could be implemented by incorporating a propagation model, although higher communications bandwidth would be necessary.

High relative precision (at megametre range) is supported by observations of apparent storm movement over a 3 km path, similar to earlier (short range) optical observations. ATD observations of tightly clustered locations are not unusual - Lee (1986a, Section 5 (c), Fig 5 and Table 2) discusses several clusters of diameter 1.7-10.7 km, where the larger clusters are observed over several minutes and show some evidence of systematic progression with time. Unfortunately these winter groupings occured over the Mediterranean sea, so detailed ground truth is not available.

ACKNOWLEDGEMENTS

My thanks are due to the Meteorologie Nationale who obtained the "ground truth" data on my behalf, and to the Special Investigations Branch of the Meteorological Office who gave patient advice on the synoptic and mesoscale interpretation of the weather observations.

REFERENCES

Kidder, R. E., 1973 The location of lightning flashes at ranges less than 100 km, J. Atmos and Terrestrial Phys., 35, 283-290.

Krider, E. P., Noggle, R. C., and Uman, M. A. 1976 A gated wideband magnetic direction finder for lightning return strokes, J. Appl. Meteor., 15, 301-306.

Lee, A. C. L. 1986a An experimental study of the remote location of lightning flashes using a VLF arrival time difference technique, London, Quart. J. Roy. Meteor. Soc., 112, 203-229.

Lee, A. C. L. 1986b An operational system for the remote location of lightning flashes using a VLF arrival time difference technique, J . Atms. Ocean. Tech., 3, 630-642.

Ludlam, F.H. 1980 Clouds and storms: the behaviour and effect of water in the atmosphere, Pennsylvania State University Press.

Master, M. J., Uman, M. A., Lin, Y. T., and Standler, R. B. 1981 Calculations of lightning return stroke electric and magnetic fields above ground, J. Geophys. Res., 86, 12127-12132.

Norrinder, H. 1954 The wave-forms of the electric field in atmospherics recorded simultaneously by two distant stations, Stockholm, Ark. Geof., 2, 161-195.

Pearson, E. S. and Hartley, H. O. 1976 Biometrica tables for statisticians, Biometrica Trust, University College, Lond.

Pierce, E. T. 1977 Lightning Volume 1 Physics of Lightning, Edited R H Golde: Chapter 10: Atmospherics and radio noise: E T Pierce, Lond, Academic Press.

Purdom, J. F. W. 1979 The development and evolution of deep convection, Preprint volume, Eleventh Conference on Severe Local Storms, October 2-5, Kansas City, Missouri, Amer. Meteor. Soc., 143-150.

Purdom, J. F. W. 1984 Use of satellite soundings and imagery for nowcasting and very-short-range forecasting, Proc. Nowcasting II Symposium (Proc. Second Int. Symposium on Nowcasting), 3-7 September, Norrkoping, Sweden, (ESA SP-208), 99-111.

Uman, M. A. 1985 Lightning return stroke electric and magnetic fields, J. Geophys. Res., 90, 6121-6130.

Watt, A. D. 1967 VLF Radio Engineering, Pergamon Press.

LIST OF FIGURE CAPTIONS

Fig 1: The meteorological situation at 1200 GMT, 12 July 1979, approximately one hour after an unusual event observed by ATD measurements at 45°04'N 03°01'E: 20 km to the east of the Plomb du Cantal. Height contours are drawn at 4000, 5000, and 6000 feet.

Fig 2: Tephigrams and wind profiles for the 1100 GMT radiosonde ascents on 12 July 1979 for Lyon, Nimes, and Bordeaux.

Fig 3: Chart depicting thunderstorms reported by ATD flash locations, meteorological observers, and lightning damage insurance claims. The Plomb du Cantal and Margeride are shown by shading bounded by contours at 1250 and 1500 m.

Fig 4: Plot of variance for the selected flashes of Table 3, normalised with respect to the variance for 12 degrees of freedom (DOF), as a function of DOF. The transition from "absolute" to "relative" location is identified by a dashed joining line.

Fig 5: Composite diagram showing an expanded view of the five ATD fixes in the ATD "event", and hodographs from the nearby radiosonde ascents. Three fixes are joined by a nominal trajectory, marked every 20 seconds, the minute marks being filled; a speed scale allows velocities to be estimated. The locations of radiosonde stations are shown relative to the ATD "event". The extremities of wind vectors from each station are drawn for levels corresponding to the numbered multiples of 100 mb. Velocity is

scaled by the filled circles for comparison with the trajectory.

Fig 6: Argand diagram representation of the complex vertical electric field of a lightning return stroke, as a function of height in meters, based on a Bruce-Golde model. Curve (a): first return stroke. Curve (b): subsequent return stroke.

OTHER INFORMATION

Suggested Short Title: Ground truth for VLF ATD fixing.

Special Symbols:

Greek letter "mu": μ

"Degrees" symbol: °

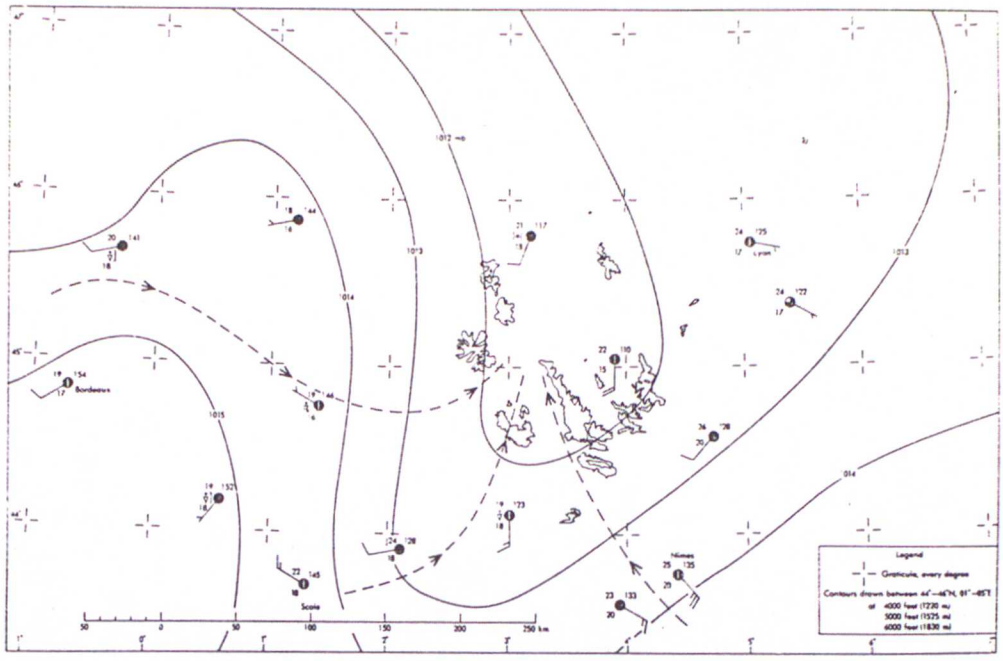

Fig 1: The meteorological situation at 1200 GMT, 12 July 1979, approximately one hour after an unusual event observed by ATD measurements at 45°04'N 03°01'E: 20 km to the east of the Plomb du Cantal. Height contours are drawn at 4000, 5000, and 6000 feet.

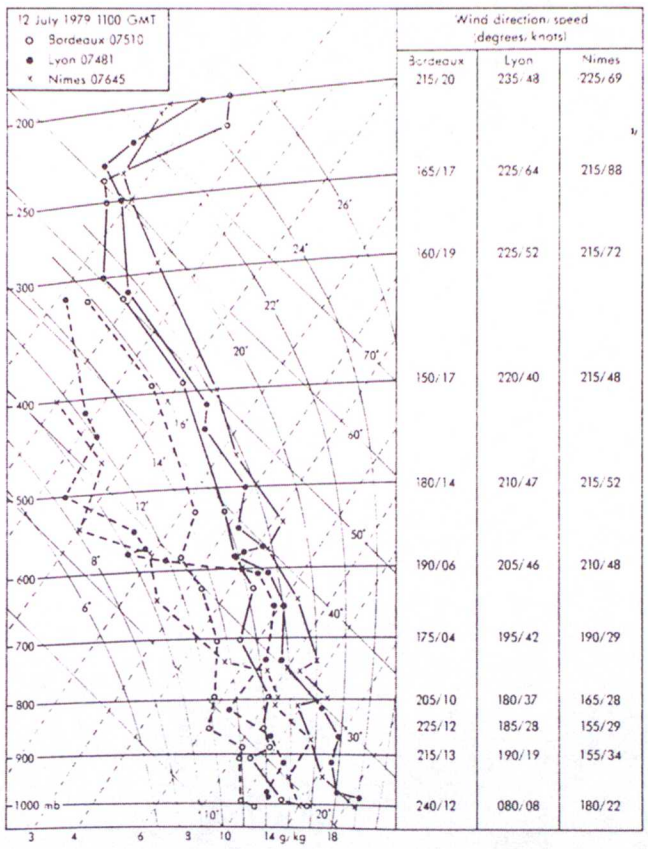

Fig 2: Tephigrams and wind profiles for the 1100 GMT radiosonde ascents on 12 July 1979 for Lyon, Nimes, and Bordeaux.

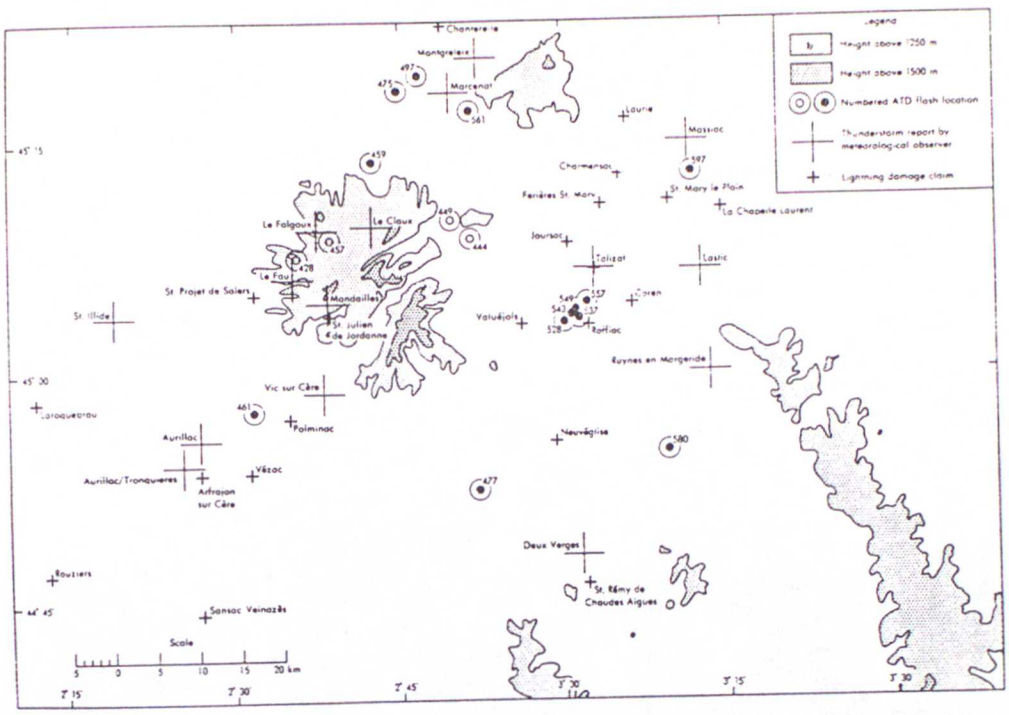

Fig 3: Chart depicting thunderstorms reported by ATD flash locations, meteorological observers, and lightning damage insurance claims. The Plomb du Cantal and Margeride are shown by shading bounded by contours at 1250 and 1500 m.

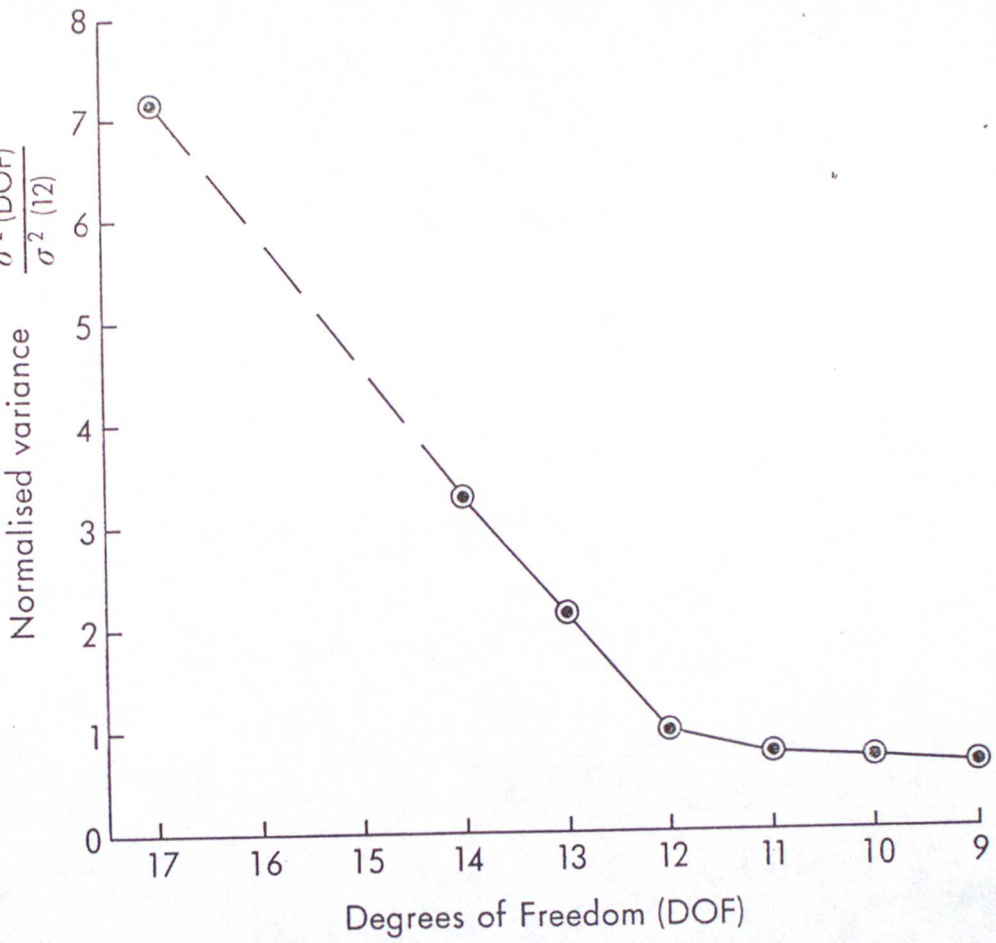

Fig 4: Plot of variance for the selected flashes of Table 3, normalised with respect to the variance for 12 degrees of freedom (DOF), as a function of DOF. The transition from "absolute" to "relative" location is identified by a dashed joining line.

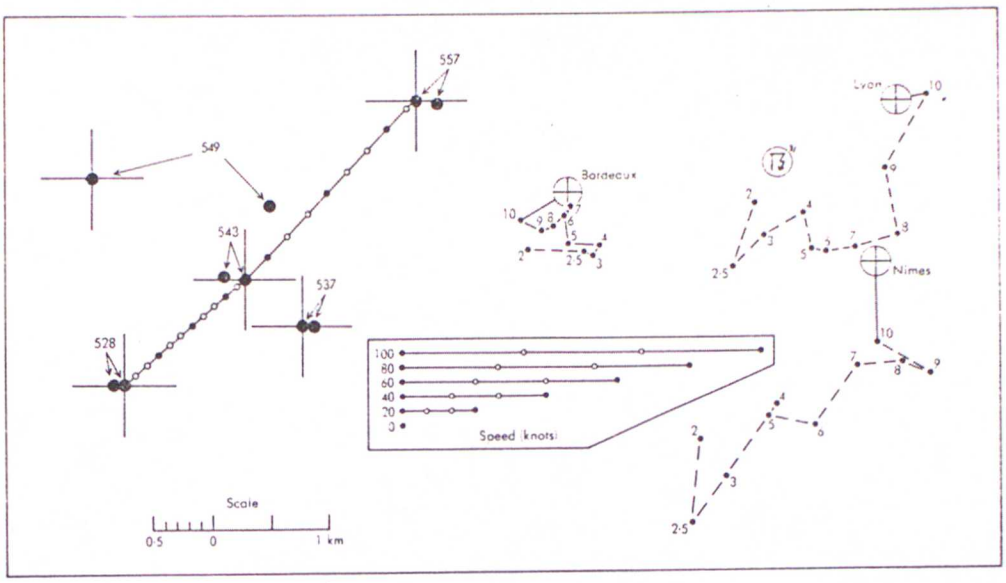

Fig 5: Composite diagram showing an expanded view of the five ATD fixes in the ATD "event", and hodographs from the nearby radiosonde ascents. Three fixes are joined by a nominal trajectory, marked every 20 seconds, the minute marks being filled; a speed scale allows velocities to be estimated. The locations of radiosonde stations are shown relative to the ATD "event". The extremities of wind vectors from each station are drawn for levels corresponding to the numbered multiples of 100 mb. Velocity is scaled by the filled circles for comparison with the trajectory.

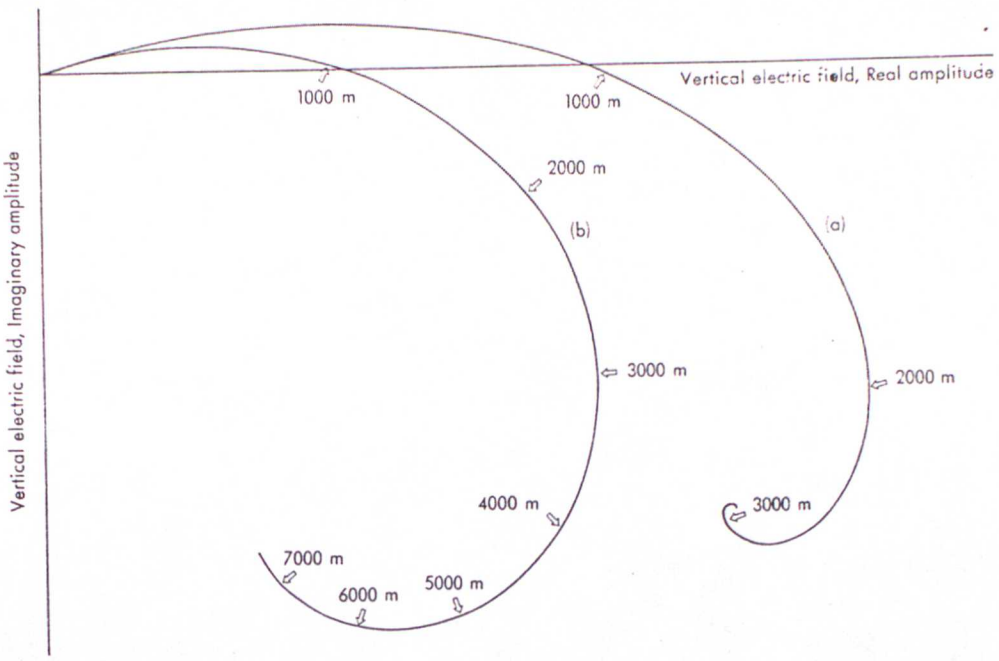

Fig 6: Argand diagram representation of the complex vertical electric field of a lightning return stroke, as a function of height in meters, based on a Bruce-Golde model. Curve (a): first return stroke. Curve (b): subsequent return stroke.